Electron-Vibrational Dynamics of Photoexcited Polyfluorenes

Ignacio Franco[†,‡] and Sergei Tretiak*[,†]

Contribution from the Theoretical Division and Center for Nonlinear Studies, Los Alamos National Laboratory, Los Alamos, New Mexico 87545, and Chemical Physics Theory Group, Department of Chemistry, University of Toronto, Toronto, Ontario M5S 3H6, Canada

Received February 25, 2004; E-mail: serg@cnls.lanl.gov

Abstract: The highly polarizable π-electron system of conjugated molecules forms the basis for their unique electronic and photophysical properties, which play an important role in numerous biological phenomena and make them important materials for technological applications. We present a theoretical investigation of the dynamics and relaxation of photoexcited states in conjugated polyfluorenes, which are promising materials for display applications. Our analysis shows that both fast ($\sim$20 fs) and slow ($\sim$1 ps) nuclear motions couple to the electronic degrees of freedom during the excited-state dynamics. Delocalized excitations dominate the absorption, whereas emission comes from localized (self-trapped) excitons. This localization is attributed to an inherent nonlinear coupling among vibronic degrees of freedom which leads to lattice and torsional distortions and results in specific signatures in spectroscopic observables. Computed vertical absorption and fluorescence frequencies as well as photoluminescence band shapes show good agreement with experiment. Finally, we demonstrate that dimerization such as spiro-linking does not affect the emission properties of molecules because the excitation becomes confined on a single chain of the composite molecule.

I. Introduction

The rich photophysics and the device applications of emissive π-conjugated polymers[1–7] arise from their highly delocalized and polarizable electronic density and the versatility in the design of their chemical structures as well as their flexibility. The evolution and relaxation of electronic excited states in these "soft" organic materials involves a complex coupled dynamics of electronic and nuclear degrees of freedom which plays an important role in many photochemical, photophysical, spectroscopic, and charge and energy transport processes. Sophisticated femtosecond spectroscopic techniques[8,9] and theoretical characterization[10,11] offer valuable insights into the nature and dynamics of these processes that could be used in the design of novel materials with improved electronic functionalities.

Conjugated polyfluorenes (PFs) and their derivatives have evolved as a major class of materials for bright blue light emission in organic light-emitting devices (OLEDs).[12–16] They exhibit an efficient electroluminescence,[17,18] high carrier mobilities,[19,20] sufficient thermal stability, and good solubility in a variety of solvents. By copolymerization[12,21–23] or doping,[24,25] it is possible to tune their emission over the entire visible spectrum. Moreover, with proper choice of side chains, these polymers exhibit liquid crystalline phases opening the possibility for polarized electroluminescence from thin film samples.[14]

The building blocks of PFs are rigid planar biphenyl units, bridged by a nonconjugated (sp[3]) carbon atom (Figures 1A and 2B). The latter can be conveniently functionalized in order to

[†] Los Alamos National Laboratory.
[‡] University of Toronto.
(1) Heeger, A. J. *Rev. Mod. Phys.* **2001**, *73*, 681–700.
(2) Friend, R. H. *Pure Appl. Chem.* **2001**, *73*, 425–430.
(3) Baldo, M. A.; Thompson, M. E.; Forrest, S. R. *Nature* **2000**, *403*, 750–753.
(4) Bernius, M. T.; Inbasekaran, M.; O'Brien, J.; Wu, W. *Adv. Mater.* **2000**, *12*, 1737–1750.
(5) Friend, R. H.; Gymer, R. W.; Holmes, A. B.; Burroughes, J. H.; Marks, R. N.; Taliani, C.; Bradley, D. D. C.; dos Santos, D. A.; Brédas, J. L.; Logdlund, M.; Salaneck, W. R. *Nature* **1999**, *397*, 121–128.
(6) Kraft, A.; Grimsdale, A. C.; Holmes, A. B. *Angew. Chem., Int. Ed.* **1998**, *37*, 402–428.
(7) Kim, D. Y.; Cho, H. N.; Kim, C. Y. *Prog. Polym. Sci.* **2000**, *25*, 1089–1139.
(8) Adachi, S.; Kobryanskii, V. M.; Kobayashi, T. *Phys. Rev. Lett.* **2002**, *89*, 027401.
(9) Lanzani, G.; Cerullo, G.; Brabec, C.; Sariciftci, N. S. *Phys. Rev. Lett.* **2003**, *90*, 047402.
(10) Brédas, J. L.; Cornil, J.; Beljonne, D.; dos Santos, D. A.; Shuai, Z. *Acc. Chem. Res.* **1999**, *32*, 267–276.
(11) Tretiak, S.; Mukamel, S. *Chem. Rev.* **2002**, *102*, 3171–3212.

(12) Muller, C. D.; Falcou, A.; Reckefuss, N.; Rojahn, M.; Wiederhirn, V.; Rudati, P.; Frohne, H.; Nuyken, O.; Becker, H.; Meerholz, K. *Nature* **2003**, *421*, 829–833.
(13) Scherf, U.; List, E. J. W. *Adv. Mater.* **2002**, *14*, 477–487.
(14) Neher, D. *Macromol. Rapid Commun.* **2001**, *22*, 1365–1385.
(15) Leclerc, M. *J. Polym. Sci., Part A: Polym. Chem.* **2001**, *39*, 2867–2873.
(16) Becker, S.; Ego, C.; Grimsdale, A. C.; List, E. J. W.; Marsitzky, D.; Pogantsch, A.; Setayesh, S.; Leising, G.; Mullen, K. *Synth. Met.* **2001**, *125*, 73–80.
(17) Pei, Q.; Yang, Y. *J. Am. Chem. Soc.* **1996**, *118*, 7416–7417.
(18) Grice, A. W.; Bradley, D. D. C.; Bernius, M. T.; Inbasekaran, M.; Wu, W. W.; Woo, E. P. *Appl. Phys. Lett.* **1998**, *73*, 629–631.
(19) Redecker, M.; Bradley, D. D. C.; Inbasekaran, M.; Woo, E. P. *Appl. Phys. Lett.* **1998**, *73*, 1565–1567.
(20) Babel, A.; Jenekhe, S. A. *Macromolecules* **2003**, *36*, 7759–7764.
(21) Cho, N. S.; Hwang, D. H.; Lee, J. I.; Jung, B. J.; Shim, H. K. *Macromolecules* **2002**, *35*, 1224–1228.
(22) Palsson, L. O.; Wang, C.; Russell, D. L.; Monkman, A. P.; Bryce, M. R.; Rumbles, G.; Samuel, I. D. W. *Chem. Phys.* **2002**, *279*, 229–237.
(23) Inbasekaran, M.; Woo, E.; Wu, W. S.; Bernius, M.; Wujkowski, L. *Synth. Met.* **2000**, *111*, 397–401.
(24) Cerullo, G.; Stagira, S.; Zavelani-Rossi, M.; De Silvestri, S.; Virgili, T.; Lidzey, D. G.; Bradley, D. D. C. *Chem. Phys. Lett.* **2001**, *335*, 27–33.
(25) Higgins, R. W. T.; Monkman, A. P.; Nothofer, H. G.; Scherf, U. *Appl. Phys. Lett.* **2001**, *79*, 857–859.

change the physicochemical properties of the polymer without compromising the electronic structure of the main conjugated backbone.[13] In dilute solutions, bulk PF samples exhibit a glassy (α) phase in which the PF chains have twisted conformations (i.e., large dihedral angles between adjacent biphenyls). During transition to the condensed state, *n*-alkyl-PFs can undergo a conformational change into a so-called β-phase in which the solid-state packing flattens the molecules into a fully planarized conformation.[13,26−28] The typical absorption spectrum of α-phase PF has a strong featureless peak at about 3.25 eV[13,14] corresponding to the ^1B_u (band gap) state absorption. The blue emission of the polymer in solution shows a well resolved vibrational structure with the 0−0 transition at 2.98 eV being the most intense.[13] β-phase formation is accompanied by a 0.1 eV red shift in the absorption and emission bands with respect to the dilute solution values.[13,26,29]

Several chemical modifications of PFs have been developed. For example, ladder-type poly(*p*-phenylene) (LPPP) is a variety of PFs the structure of which is chemically enforced to be planar (Figure 2B). Its spectroscopic similarities with β-phase PF are often used to justify a planar structure for the β conformation.[13] Since in solid-state samples molecular aggregation and/or excimer formation may strongly affect the photophysical properties of the devices introducing instability in the emission spectra,[30−36] spiro-linked PFs (Figure 6B) have become an important way to prevent π-stacking and, thus, to stabilize the blue emission of PF films.

Due to the technological importance of PFs, a theoretical analysis of their electronic structure, behavior of spectroscopic observables, and the role of disorder and defects is of current topical interest. Previous quantum chemical studies have focused on the effect of doping with Li atoms,[37] the influence of copolymerization on the absorption spectra,[38] and the role of keto defects on the absorption and emission properties.[39,40] The latter showed that keto defects introduce a yellow-green parasite emission band, traditionally assigned to aggregate formation, that changes the desired blue emission of the polymer into a green color. The origin of this low-energy emission band has

been extensively studied experimentally as well.[41−44] Despite the considerable theoretical effort[37−40] in characterizing the properties of PFs, many important issues related to the nature, dynamics, and relaxation of photoexcitations in these polymers have not been addressed yet. For this reason, here we report a quantum chemical investigation of the adiabatic photoexcited dynamics, absorption, and emission properties of PFs. Ground and excited electronic state equilibrium geometries and the photoexcited dynamics are computed using the recently developed excited-state molecular dynamics (ESMD) approach.[45] The simulations are performed by combining the Austin Model 1 (AM1) semiempirical Hamiltonian with the collective electronic oscillator (CEO) representation.[11] The computational results are further analyzed in terms of geometric (dihedral angles and bond length alternation) variables to follow the nuclear dynamics and transition densities, natural transition orbitals, and spectroscopic parameters to monitor the electronic dynamics.

The details of our computational approach are discussed in section II.A. Section II.B introduces a real-space analysis of the spatial evolution of photoexcitations, in terms of transition densities and orbitals, that is used throughout this work. In section III.A we study the photoexcited dynamics of LPPP and PF oligomers (in the glassy (α) and planar (β) conformations) of different lengths. In section III.B we focus on the effect of dimerization (spiro-linking) on the photophysical properties of PFs. Similar molecules have been recently synthesized and characterized by Katzis et al..[30] Finally, we discuss the trends that emerge and summarize our results in section IV.

II. Theoretical Methodology

A. Computational Approach. To study absorption and emission properties of PF-type oligomers as well as their photoexcited dynamics, we employed the following computational strategy. Ground-state optimal geometries were obtained using the Austin Model 1 (AM1) semiempirical Hamiltonian[46] at the Hartree−Fock (HF) level. The AM1 approach was specifically designed for this purpose. The vertical transition frequencies from the ground state to the excited states were then calculated with the CEO procedure[11] combined with the AM1 or the intermediate neglect of differential overlap/spectroscopy (INDO/S) Hamiltonian.[47,48] The latter was specifically parametrized for computing UV−visible spectra of organic molecules. The CEO approach, described in detail elsewhere (e.g., refs 11 and 49), solves the equation of motion for the single-electron density matrix[50]

$$\rho_{mn}(t) = \langle \Psi(t) | c_m^\dagger c_n | \Psi(t) \rangle \qquad (1)$$

of a molecule driven by an external electric field using a time-dependent Hartree−Fock (TDHF) approximation for the many-electron problem.[51,52] Here $|\Psi(t)\rangle$ is the many-electron wave function (time-dependent

(26) Winokur, M. J.; Slinker, J.; Huber, D. L. *Phys. Rev. B* **2003**, *67*, 184106.
(27) Grell, M.; Bradley, D. D. C.; Ungar, G.; Hill, J.; Whitehead, K. S. *Macromolecules* **1999**, *32*, 5810−5817.
(28) Grell, M.; Bradley, D. D. C.; Long, X.; Chamberlain, T.; Inbasekaran, M.; Woo, E. P.; Soliman, M. *Acta Polym.* **1998**, *49*, 439−444.
(29) Ariu, M.; Sims, M.; Rahn, M. D.; Hill, J.; Fox, A. M.; Lidzey, D. G.; Oda, M.; Cabanillas-Gonzalez, J.; Bradley, D. D. C. *Phys. Rev. B* **2003**, *67*, 195333.
(30) Katsis, D.; Geng, Y. H.; Ou, J. J.; Culligan, S. W.; Trajkovska, A.; Chen, S. H.; Rothberg, L. J. *Chem. Mater.* **2002**, *14*, 1332−1339.
(31) Setayesh, S.; Grimsdale, A. C.; Weil, T.; Enkelmann, V.; Mullen, K.; Meghdadi, F.; List, E. J. W.; Leising, G. *J. Am. Chem. Soc.* **2001**, *123*, 946−953.
(32) Klarner, G.; Lee, J. I.; Davey, M. H.; Miller, R. D. *Adv. Mater.* **1999**, *11*, 115−119.
(33) Marder, S. R.; Kippelen, B.; Jen, A. K. Y.; Peyghambarian, N. *Nature* **1997**, *388*, 845−851.
(34) Martin, R. E.; Diederich, F. *Angew. Chem., Int. Ed.* **1999**, *38*, 1350−1377.
(35) Miteva, T.; Meisel, A.; Knoll, W.; Nothofer, H. G.; Scherf, U.; Muller, D. C.; Meerholz, K.; Yasuda, A.; Neher, D. *Adv. Mater.* **2001**, *13*, 565−570.
(36) Nguyen, T. Q.; Martini, I. B.; Liu, J.; Schwartz, B. J. *J. Phys. Chem. B* **2000**, *104*, 237−255.
(37) Greczynski, G.; Fahlman, M.; Salaneck, W. R.; Johansson, N.; dos Santos, D. A.; Dkhissi, A.; Brédas, J. L. *J. Chem. Phys.* **2002**, *116*, 1700−1706.
(38) Cornil, J.; Gueli, I.; Dkhissi, A.; Sancho-Garcia, J. C.; Hennebicq, E.; Calbert, J. P.; Lemaur, V.; Beljonne, D.; Bredas, J. L. *J. Chem. Phys.* **2003**, *118*, 6615−6623.
(39) Franco, I.; Tretiak, S. *Chem. Phys. Lett.* **2003**, *372*, 403−408.
(40) Zojer, E.; Pogantsch, A.; Hennebicq, E.; Beljonne, D.; Bredas, J. L.; Scanducci de Freitas, P.; Scherf, U.; List, E. J. W. *J. Chem. Phys.* **2002**, *117*, 6794−6802.

(41) Gong, X.; Iyer, P. K.; Moses, D.; Bazan, G. C.; Heeger, A. J.; Xiao, S. S. *Adv. Funct. Mater.* **2003**, *13*, 325−330.
(42) Nikitenko, V. R.; Lupton, J. M. *J. Appl. Phys.* **2003**, *93*, 5973−5977.
(43) Lupton, J. M.; Craig, M. R.; Meijer, E. W. *Appl. Phys. Lett.* **2002**, *80*, 4489−4491.
(44) List, E. J. W.; Guentner, R.; Scanducci de Freitas, P.; Scherf, U. *Adv. Mater.* **2002**, *14*, 374−378.
(45) Tretiak, S.; Saxena, A.; Martin, R. L.; Bishop, A. R. *Phys. Rev. Lett.* **2002**, *89*, 097402.
(46) Dewar, M. J. S.; Zoebisch, E. G.; Healy, E. F.; Stewart, J. J. P. *J. Am. Chem. Soc.* **1985**, *107*, 3902−3909.
(47) Ridley, J.; Zerner, M. C. *Theor. Chim. Acta* **1973**, *32*, 111−134.
(48) Karlsson, G.; Zerner, M. C. *Int. J. Quantum Chem.* **1973**, *7*, 35−49.
(49) Mukamel, S.; Tretiak, S.; Wagersreiter, T.; Chernyak, V. *Science* **1997**, *277*, 781−787.
(50) Davidson, E. R. *Reduced Density Matrices in Quantum Chemistry*; Academic Press: New York, 1976.
(51) Thouless, D. J. *The Quantum Mechanics Of Many-Body Systems*; Academic Press: New York, 1972.

single Slater determinant driven by an external field), $c_m^\dagger$ (c_m) are creation (annihilation) operators, and the indices m and n refer to known basis functions (e.g., atomic orbitals, AOs, in the site representation). Within this theoretical framework, the changes induced in the density matrix by an external field are expressed as linear combinations of the electronic transition densities $\{\xi_\eta\}$.[11,49] These are defined as

$$(\xi_\eta)_{mn} = \langle \eta | c_m^\dagger c_n | g \rangle \tag{2}$$

and reflect the changes in the electronic density induced by an optical transition from the ground state $|g\rangle$ to an excited state $|\eta\rangle$. The transition densities (or electronic modes) are, in turn, the eigenfunctions of the two-particle Liouville operator L from the linearized TDHF equation of motion[11,51−53]

$$L\xi_\eta = \Omega_\eta \xi_\eta, \tag{3}$$

where the eigenvalues Ω_η are electronic $|g\rangle \rightarrow |\eta\rangle$ transition energies. The eigenvalue problem stated in eq 3 may be written in matrix form as[11,51,54]

$$\begin{pmatrix} A & B \\ -B & -A \end{pmatrix} \begin{bmatrix} X \\ Y \end{bmatrix} = \Omega \begin{bmatrix} X \\ Y \end{bmatrix}, \tag{4}$$

which is known as the first-order random phase approximation (RPA) eigenvalue equation.[11,53] Here X and Y are particle-hole and hole-particle components of the transition density $\xi = \begin{bmatrix} X \\ Y \end{bmatrix}$ in the molecular orbital (MO) representation, respectively. The matrix A is Hermitian and identical to the configuration interaction (CI) singles matrix (CI singles is also known as the Tamm−Dancoff approximation), whereas the Hermitian matrix B represents higher order electronic correlations included in the TDHF approximation and it is known as the de-excitation operator. The direct diagonalization of L in eq 4 is the potential computational bottleneck of the excited state calculations. The CEO procedure circumvents this problem using numerically efficient Krylov space algorithms (e.g., Lanczos or Davidson).[11,55−58] This is possible since the action of the TDHF operator L on an arbitrary single electron matrix ξ can be calculated on the fly without constructing and storing the full matrix L in memory (direct approach).[11,57,58] Subsequently the computation of excited states is not substantially more numerically demanding than the ground-state calculations.

The TDHF approximation accounts for essential electronic correlations (electron−hole interactions plus some additional higher order terms)[51,52,59] which is sufficient for reasonably accurate calculations of UV−visible spectra in many extended organic molecular systems.[11] It has the advantage of being size consistent, a major failure of truncated CI techniques.[60] However, excited states with a significant double excitation character (e.g., A_g states in polyacetylene) cannot be represented accurately with the TDHF and CI singles methods.[61] We also note that the TDHF approximation uses the HF ground state as a reference state. If this state does not correspond to a stable minimum (a positive energy Hessian) and if the electronic correlations (doubles and higher orders) are significant for the ground-state wave function, the first-order RPA approximation breaks down and eq 4 may yield imaginary eigenvalues.[62−67] For example, large contributions from

doubly excited configurations lead to imaginary RPA energies of triplet states in both ethylene and formaldehyde.[68,69] Extended conjugated molecules, like the ones studied in this contribution, have stable HF ground states (closed shell) and small second-order electronic correlations. For these reasons, the approximations used in the CEO approach are well suited for computing their electronic excitations contributing to UV−visible spectra.[11] Since the norm of the matrix B is typically small for singlet states in extended conjugated systems, the results that we obtain are similar to those of CI singles. In general RPA gives better results compared to CI singles (in particular for transition dipoles and oscillator strengths).[70−72]

The evolution of the molecules after initial photoexcitation is followed using the ESMD approach,[45] which calculates classical nuclear trajectories on the excited-state adiabatic potential energy hypersurface. A schematic representation of the computations presented herein is shown in Figure 2A: an oligomer, initially in the ground-state optimal geometry, is photoexcited (vertical absorption Ω_A) by creating an electron−hole pair (exciton). This initial photoexcitation (hot exciton) is allowed to evolve along the molecular excited-state potential energy surface $E_e(\mathbf{q})$ according to the Newtonian equations of motion for the nuclear degrees of freedom

$$M_\alpha \frac{\partial^2 q_\alpha}{\partial t^2} + b \frac{\partial q_\alpha}{\partial t} = F_\alpha = -\frac{\partial E_e(\mathbf{q})}{\partial q_\alpha}, \qquad \alpha = 1, \cdots, 3N-6 \quad (5)$$

using a numerical velocity Verlet finite difference algorithm.[73] Here q_α and M_α represent the coordinates and the mass of one of the $3N-6$ vibrational normal modes (N being the total number of atoms in the molecule). The forces F_α are obtained as numerical derivatives of the exited-state energy $E_e(\mathbf{q})$ with respect to q_α (as opposed to analytical derivative techniques[74] which are also feasible).[74] We follow the dynamics of all $(3N-6)$ nuclear degrees of freedom of the molecule. The excited-state potential energy surface $E_e(\mathbf{q})$ and the forces that enter into eq 5 are calculated quantum mechanically using the CEO method. Namely, for each nuclear configuration $\mathbf{q}$, $E_e(\mathbf{q}) = E_g(\mathbf{q}) + \Omega_\eta(\mathbf{q})$. The ground-state energy $E_g(\mathbf{q})$ is obtained at the AM1/HF level; the vertical $|g\rangle \rightarrow |\eta\rangle$ transition frequency $\Omega_\eta(\mathbf{q})$ is calculated with the CEO technique combined with the AM1 model. Using the same Hamiltonian model (AM1) for both ground and excited states results in a significant computational simplification that, together with efficient Davidson diagonalization[55,57,58] techniques, makes it possible to follow picosecond excited-state dynamics of quite large (200−300 atoms) molecular systems taking into account all their $3N-6$ vibrational degrees of freedom. In the dynamics, we focus on the lowest singlet excited ^1B_u band gap state ($\Omega_\eta = \Omega_1 = \Omega$) as it is the most important one in the UV−visible spectra of conjugated polymers. The simulations allow us to follow the gas-phase dynamics with vanishing damping ($b = 0$) or in an effective viscous medium ($b \neq 0$). The latter leads to the excited state optimal geometry which is obtained by letting the propagation to run sufficiently long for equilibration to occur. From this configuration, the resulting "cold exciton" decays radiatively back to the ground state (vertical fluorescence Ω_F in Figure 2A). The present calculations neglect the effects of the surrounding dielectric media which, however, could

(52) Ring, P.; Schuck, P. *The Nuclear Many-Body Problem*; Springer-Verlag: New York, 1980.
(53) Linderberg, J.; Jorgensen, P.; Oddershede, J.; Ratner, M. *J. Chem. Phys.* **1972**, *56*, 6213−19.
(54) Linderberg, J.; Öhrn, Y. *Propagators in Quantum Chemistry*; Academic Press: London, 1973.
(55) Davidson, E. R. *J. Comput. Phys.* **1975**, *17*, 87−94.
(56) Weiss, H.; Ahlrichs, R.; Häser, M. *J. Chem. Phys.* **1993**, *99*, 1262−1270.
(57) Rettrup, S. *J. Comput. Phys.* **1982**, *45*, 100−107.
(58) Stratmann, R. E.; Scuseria, G. E.; Frisch, M. J. *J. Chem. Phys.* **1998**, *109*, 8218−8224.
(59) Pines, D.; Bohm, D. *Phys. Rev.* **1952**, *85*, 338−353.
(60) Szabo, A.; Ostlund, N. S. *Modern Quantum Chemistry: Introduction to Advanced Electronic Structure Theory*; McGraw-Hill: New York, 1989.
(61) Hirata, S.; Head-Gordon, M.; Bartlett, R. J. *J. Chem. Phys.* **1999**, *111*, 10774−10786.
(62) Shibuya, T.-I.; McKoy, V. *Phys. Rev. A* **1970**, *2*, 2208−2218.

(63) Jorgensen, P.; Oddershede, J.; Ratner, M. A. *Chem. Phys. Lett.* **1975**, *32*, 111−115.
(64) Oddershede, J.; Jorgensen, P. *J. Chem. Phys.* **1977**, *66*, 1541−1556.
(65) Paldus, J.; Čížek, J. *J. Chem. Phys.* **1974**, *60*, 149−163.
(66) Öhrn, Y.; Linderberg, J. *Int. J. Quantum Chem.* **1979**, *15*, 343−353.
(67) Linderberg, J. *Phys. Scripta* **1980**, *21*, 373−377.
(68) Dunning, T. H.; McKoy, V. *J. Chem. Phys.* **1967**, *47*, 1735.
(69) Dunning, T. H.; McKoy, V. *J. Chem. Phys.* **1967**, *48*, 5263.
(70) Baker, J. D.; Zerner, M. C. *J. Phys. Chem.* **1991**, *95*, 8614−8619.
(71) Baker, J. D.; Zerner, M. C. *Chem. Phys. Lett.* **1990**, *175*, 192−196.
(72) Parkinson, W. A.; Zerner, M. C. *Chem. Phys. Lett.* **1987**, *139*, 563−570.
(73) Allen, M. P.; Tildesley, D. J. *Computer Simulation of Liquids*; Clarendon Press: Oxford, 1987.
(74) Furche, F.; Ahlrichs, R. *J. Chem. Phys.* **2002**, *117*, 7433−7447.

be taken into account in the ESMD method using an appropriate solvation model.[75,76]

The excited and ground-state equilibrium geometries obtained with the ESMD approach may be used for calculating the absorption and emission band shapes within the Condon approximation for displaced (in conformational space) multidimensional harmonic oscillators.[77,78] The distribution of the transition probabilities from the excited-state relaxed conformation to the various vibrational modes of the ground state is modeled by convolutions of Lorentzian line shapes, multiplied by Franck−Condon factors. Consequently, the imaginary part of the polarizability (which determines the fluorescence band shape) as a function of the frequency ω is given in the zero-temperature limit by[77,78]

$$\alpha(\omega) = \text{Im}\left\{\mu^2 \sum_{\nu_1}\cdots\sum_{\nu_{3N-6}} \frac{\prod_{n=1}^{3N-6}\langle 0|\nu_n\rangle^2}{\Omega^{(0)} - \sum_{n=1}^{3N-6}\nu_n\omega_n - \omega - i\Gamma}\right\}. \quad (6)$$

Here μ is the electronic transition dipole moment between the excited and the ground states, and $\Omega^{(0)}$ is the associated 0−0 transition energy; ω_n and ν_n are the vibrational frequencies and quanta of the participating normal modes, respectively. The vibrational overlap integrals (Franck−Condon factors)

$$\langle 0|\nu_n\rangle^2 = \frac{e^{-S_n}S_n^\nu}{\nu!} \quad (7)$$

depend on the dimensionless displacements Δ_n of each normal mode and conform to a Poisson distribution with Huang−Rhys factors $S_n = \Delta_n^2/2$. The line width Γ is the only empirical parameter required for modeling the vibronic spectra. It affects the shape of the vibrational features and the relative intensities of the corresponding peaks. For all calculations, we used $\Gamma = 0.03$ eV to resolve the main vibrational progression and to simultaneously coarse grain over the low-frequency normal modes. We used Lorentzian line shapes in eq 6 because our computations reflect the spectroscopic properties of a single isolated molecule the spectra of which are typically homogeneously broadened. We note that computed AM1 vibrational frequencies are systematically overestimated as it is a typical case for semiempirical computations. As a consequence, the predicted vibrational tailing of the emission bands is somewhat larger than the ones observed in experiments.

B. Transition Densities and Natural Transition Orbitals (NTOs). During the photoexcited dynamics the molecular geometry gets distorted and this, in turn, induces strong changes in the electronic wave function. To connect these structural changes with the distinct dynamics of the underlying photoinduced electron−hole pairs, we use a two-dimensional real-space analysis[11,49] and a natural transition orbital decomposition[79] of the calculated transition densities ξ_η (eq 2).

The diagonal elements of the transition densities $(\xi_\eta)_{nn}$ represent the net charge induced in the n-th AO by an external field. The off-diagonal elements $(\xi_\eta)_{mn}$ ($m \neq n$) represent the joint probability amplitude of finding an electron and a hole located on the m-th and n-th AOs, respectively. To obtain a two-dimensional real-space display of these modes, we coarse grain them over the various orbitals belonging to each atom. In practice, the hydrogens are omitted because they weakly participate in the delocalized electronic excitations. For other atoms we use the following contraction: the total induced charge on each atom A is given by

(75) Moran, A. M.; Kelley, A. M.; Tretiak, S. *Chem. Phys. Lett.* **2003**, *367*, 293−307.
(76) Klamt, A.; Schuurmann, G. *J. Chem. Soc., Perkin Trans. 2* **1993**, *5*, 799−805.
(77) Myers, A. B.; Mathies, R. A.; Tannor, D. J.; Heller, E. J. *J. Chem. Phys.* **1982**, *77*, 3857−3866.
(78) Karabunarliev, S.; Baumgarten, M.; Bittner, E. R.; Mullen, K. *J. Chem. Phys.* **2000**, *113*, 11372−11381.
(79) Martin, R. L. *J. Chem. Phys.* **2003**, *118*, 4775−4777.

$$(\xi_\eta)_A = |\sum_{n_A}(\xi_\eta)_{n_A n_A}|, \quad (8)$$

whereas an average over all off-diagonal matrix elements represents the effective electronic coherence between atoms A and B,

$$(\xi_\eta)_{AB} = \sqrt{\sum_{n_A m_B}[(\xi_\eta)_{n_A m_B}]^2}. \quad (9)$$

Here the indices n_A and m_B run over all atomic orbitals localized on atoms A and B, respectively. The size of the resulting matrix $(\xi_\eta)_{AB}$ is now equal to $N' \times N'$, N' being the number of atoms in the molecule without hydrogens. Contour plots of $(\xi_\eta)_{AB}$ provide a real-space picture of electronic transitions by showing accompanying motions of optically induced charges and electronic coherences.[11,49] Two characteristic lengths are of relevance in these plots. The diagonal size of the nonzero matrix elements L_d reflects the degree of localization of the optical excitation (the position of the center of mass of the electron−hole pair). The largest off-diagonal extent of the nonzero matrix area (coherence length L_c) measures the maximal distance between the electron and hole (the exciton size).

The NTOs[79] constitute an alternative and complementary representation of the electronic transitions. They offer the most compact representation of a given transition density in terms of an expansion into single-particle transitions. The NTOs are obtained by using the orbital transformation of Amos and Hall[79,80]

$$(\phi_1,\phi_2,...,\phi_{K_o}) = (\psi_1,\psi_2,...,\psi_{K_o})\mathbf{U}, \quad (10)$$

$$(\phi'_1,\phi'_2,...,\phi'_{K_v}) = (\psi'_1,\psi'_2,...,\psi'_{K_v})\mathbf{V}, \quad (11)$$

where ψ_i ($i = 1,..., K_o$) and ψ_j ($j = 1,..., K_v$) denote occupied and unoccupied molecular orbitals (MOs) and indices i and j run over the occupied and unoccupied subspaces, respectively. ϕ_i (ϕ'_j) is the new set of occupied (unoccupied) natural transition orbitals resulting from this transformation. In turn, $\mathbf{U}$ and $\mathbf{V}$ are calculated by diagonalizing the particle-hole block of the transition density ξ_{ph} of a given electronic state (a rectangular $K_o \times K_v$ matrix in MO representation) as

$$\xi_{ph}\xi_{ph}^\dagger u_i = \lambda_i u_i, \quad \mathbf{U} = (u_1, u_2,..., u_{K_o}), \quad (12)$$

$$\xi_{ph}^\dagger\xi_{ph} v_j = \lambda'_j v_j, \quad \mathbf{V} = (v_1, v_2,..., v_{K_v}). \quad (13)$$

The transition density matrix ξ_{ph} is diagonal in this representation

$$|(\mathbf{U}^\dagger\xi_{ph}\mathbf{V})_{ij}| = \sqrt{\lambda_i}\delta_{ij}; \quad (14)$$

the resulting eigenvalues λ measure the contribution of each "electron−hole" NTO pair to the transition density ξ_{ph}. Numbered in order of decreasing magnitude, they obey: $1 \geq \lambda_i \equiv \lambda'_i \geq 0$ (for $i = 1, ..., K_o$), $\lambda'_j = 0$ (for $j = K_o + 1, ..., K_v$), and $\Sigma_{i=1}^{K_o} \lambda_i \approx 1$.[79] The resulting quasiparticle basis set of NTOs $\{\phi,\phi'\}_\eta$ for the transition density ξ_η offers a compact representation of a given electronic transition $|g\rangle \rightarrow |\eta\rangle$ in terms of new single-particle orbitals. For example, $\lambda_1 = 1$ means that the excited state can be well represented as a transition between two orbitals, whereas several nonzero eigenvalues λ indicate that the excitation is an irreducible mixing of different electronic configurations. The NTOs thus facilitate the interpretation of the true nature of the excited state in contrast to the usual analysis in terms of a set of MOs which, typically, contains many equally dominant configurations.

To illustrate the NTO and transition density real-space analysis we consider an example. Figure 1 shows the dominant NTOs and the coarse-grained transition densities for the first two excited states of a PF oligomer with a keto defect in one of the extremes (Figure 1A). A

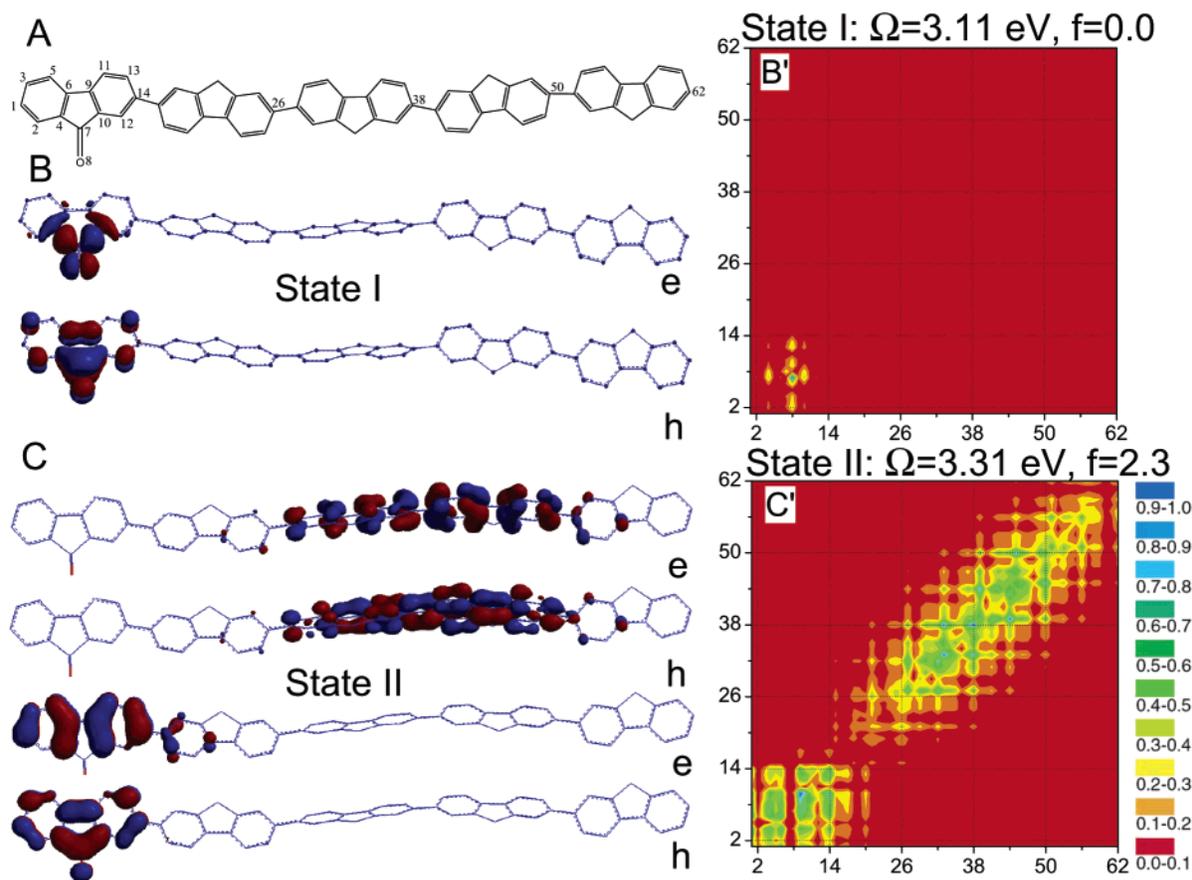(80) Amos, A. T.; Hall, G. G. *Proc. R. Soc. London* **1961**, *A263*, 483−493.

Figure 1. Natural transition orbital (NTO) decomposition and two-dimensional real space analysis of the electronic transition densities from the ground state to the first two excited states of the PF oligomer with a keto defect shown in part A. (B and C) Electron (e) and hole (h) NTOs with the highest contributions to the electronic transition density matrices. The associated weights (eigenvalues λ) for each NTO pair (from top to bottom) are 0.992, 0.510, and 0.400. (B′ and C′) Contour plots of the transition density matrices corresponding to transitions to state I and II. The axes label atoms along the oligomer in the numbering sequence shown in part A. Each plot depicts probabilities of an electron moving from one molecular position (horizontal axis) to another (vertical axis) upon electronic excitation. The color code is given in the lower-right corner of the figure.

detailed theoretical study of the electron-vibrational relaxation of photoexcited polyfluorenes in the presence of chemical defects is given in ref 39. The first excited state (I) is completely localized around the carbonyl group as shown in the contour plot of the corresponding transition density (Figure 1B′). Even though several MO pairs contribute to this transition (the weight of the dominant MO pair is 0.64), state I can be compactly represented by a single pair of NTOs (Figure 1B) with weight $\lambda = 0.992$. In close agreement with the transition density contour plots, both "electron" and "hole" NTOs for state I are localized around the carbonyl group. In contrast, state II corresponding to the band gap ^1B_u excitation is delocalized along the pristine part of the molecule with some participation of the unit with the keto defect (Figure 1C′). Many MO pairs contribute to the state II transition. However, it can be decomposed into only two dominant pairs of NTOs localized on the bulk chain and on the fluorenone unit (Figure 1C). We note that NTOs only reflect changes in the electronic density upon photoexcitation; the off-diagonal elements of the transition density, associated with the photoinduced coherences, cannot be directly represented in such orbital construct. However, they are closer in spirit to the usual quantum-chemical orbital analysis upon which the traditional chemical intuition is built. Subsequently, NTOs and two-dimensional plots of the transition densities constitute complementary real-space analysis to interpret changes in the electronic structure induced by an optical excitation.

III. Results and Discussion

A. Photoexcited Dynamics of PFs. We start by investigating the structural and spectroscopic differences of PF and LPPP

oligomers at absorption and emission (Figure 2). The corresponding theoretical and experimental values for the transition frequencies and oscillator strengths are presented in Table 1. Hereafter we will refer to the α-type PF oligomer with n fluorene units as α-PF(n), and in a similar fashion, the β-type and LPPP oligomers will be called β-PF(n) and LPPP(n), respectively. For characterizing geometrical changes induced by photoexcitation in the oligomers, we use dihedral angles and bond length alternation parameters. Dihedral angles are defined as the deviation from 180° of the torsional angle between the neighboring fluorene units around the bond that connects them. Small dihedral angles (i.e., planar structures) promote the delocalization of the π-electron system. Similarly, the bond length alternation parameter provides a quantitative measure of the homogeneity in the distribution of π electrons over the bonds (Peierls distortion) by comparing the length of consecutive bonds along the chain. An enhancement in the electronic delocalization tends to equalize the bond lengths and thus reduces the bond length alternation. Both parameters depend on the chemical substituents, solvent effects, and other environmental factors.

The ground state of α-PF(5) is not planar (Figure 2C). Steric interactions between the neighboring fluorene units result in a twisted configuration with an $\sim$41° dihedral angle between monomers, which agrees well with the experimental value of $\sim$36°.[13] When going to the excited ^1B_u state, α-PF(5) acquires
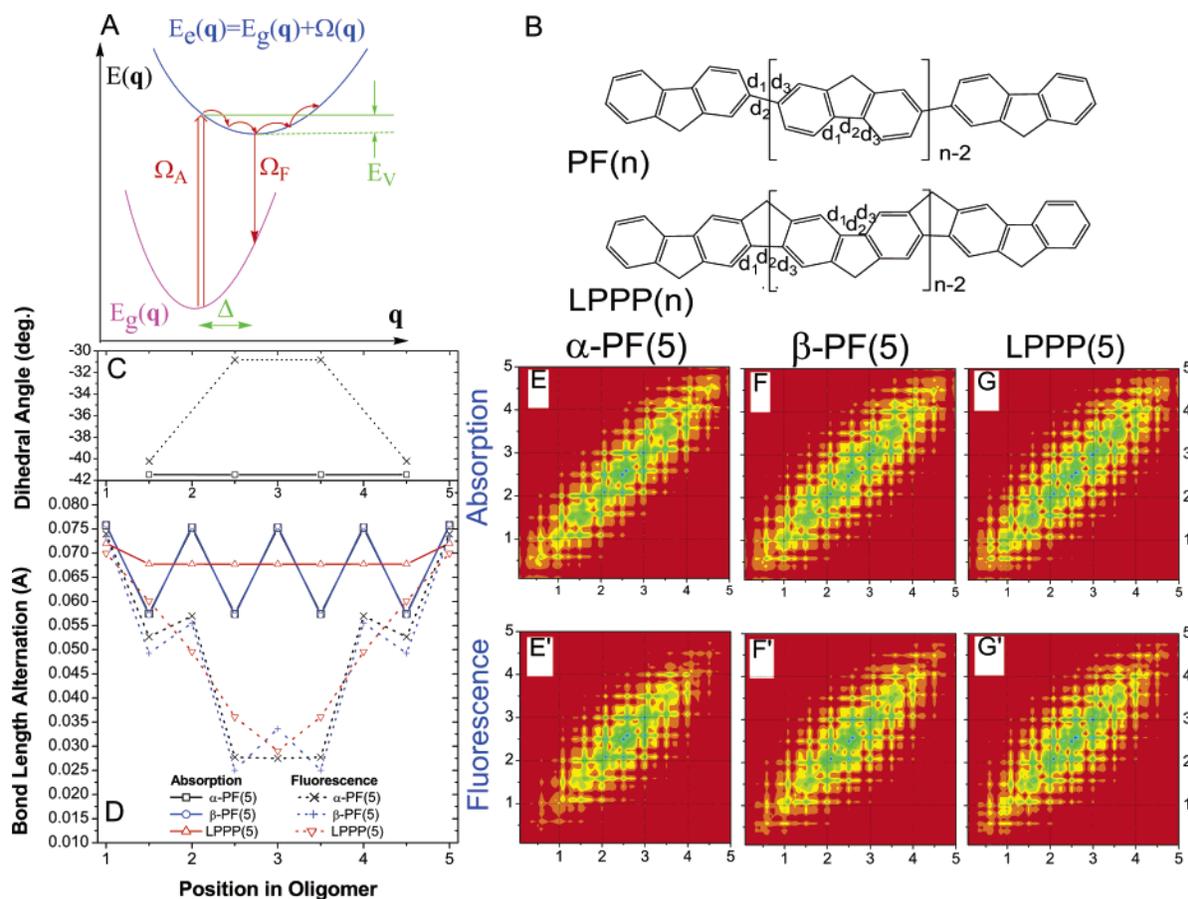
Figure 2. (A) Schematic representation of the photoexcited dynamics. Ω_A and Ω_F are vertical absorption and fluorescence transition energies, respectively; $E_g(\mathbf{q})$ and $E_e(\mathbf{q})$ represent the energy as a function of nuclear coordinates $\mathbf{q}$, displacements Δ and vibrational reorganization energy E_V, for the ground and excited states, respectively. (B) Structure of polyfluorene (PF) and planarized PPP-type ladder polymers. Variation of (C) dihedral angles and (D) bond length alternation parameters (defined as $d_2 - (d_1 + d_3)/2$ as shown in part B)) along the oligomer chain for the ground and excited-state relaxed geometries in α- and β-phase PF(5) and LPPP(5). The X-axis labels consecutive monomers (half-integers correspond to the positions between monomers) as shown in part B. The lower-right panel shows contour plots of the transition density matrices at the moment of absorption and emission. Parts E−G show transitions from the ground-state equilibrium geometry to the lowest excited state and correspond to the vertical absorption. Parts E′−G′ represent the same quantities as those in parts E−G but computed at the excited-state equilibrium geometries and correspond to the vertical fluorescence. The axes label repeat units (n) in the oligomers. The color code is shown in Figure 1.

Table 1. Computed Vertical Absorption Ω_A (Band Gap) and Fluorescence Ω_F Transition Energies for α- and β-Phase PFs, LPPP, and γ and Spiro-γ Oligomer Chains[a]

	calculations				experiment	
	INDO/S		AM1			
	Ω_A (eV)	Ω_F (eV)	Ω_A (eV)	Ω_F (eV)	Ω_A (eV)	Ω_F (eV)
α-PF(5)	3.25 (3.5)	2.94 (3.1)	2.90 (2.1)	2.63 (2.0)	3.2−3.3	2.98/2.80/2.60
β-PF(5)	3.01 (3.7)	2.78 (3.5)	2.72 (2.3)	2.51 (2.3)	3.22/3.04/2.85	2.81/2.65/2.49
LPPP(5)	2.90 (3.5)	2.68 (3.3)	2.62 (2.0)	2.42 (2.0)	3.12/2.95/2.75	2.71/2.55/2.39
γ	3.30 (2.6)	2.94 (2.4)	2.94 (1.6)	2.63 (1.6)		
Spiro-γ(I)	3.27 (2.0)	2.91 (2.2)	2.93 (1.3)	2.61 (1.5)		
Spiro-γ(II)	3.27 (2.7)	3.26 (2.4)	2.93 (1.7)	2.93 (1.5)		

[a] States I and II in the Spiro-γ dimer correspond to the first two excited states. The associated oscillator strengths are given in parentheses. Experimental values correspond to the vibrational peaks in the absorption/emission spectra reported in ref 13.

a more planar conformation in the middle of the molecule improving π conjugation between the three inner fluorene units (Figure 2C). β-phase PF and LPPP remain planar when going to the excited state. The bond length alternation in the ground state geometry of all three oligomers is constant for equivalent bonds along the chains, and noticeably reduced in the middle of the molecule for the ^1B_u excited-state geometries. This localized reduction of dihedral angles and bond length alternations is a characteristic signature of confinement of the excitation by vibrational relaxation (exciton self-trapping[45]).

To connect these structural changes with the underlying dynamics of electron−hole pairs, we use two-dimensional real-space analysis of the transition densities (section II.B) computed at the ground (absorption) and excited (fluorescence) state geometries (Figure 2). In the three oligomers, the excitation created by ^1B_u state absorption (Figure 2E−G) is delocalized over the entire chain. In α-PF(5) the exciton size (off-diagonal extend L_c) is about 2 repeat units, while in β-PF(5) and LPPP-(5) it is slightly larger due to the greater extent of π conjugation induced by their planar structures. Spectroscopically, this

Table 2. Geometrical Differences between the Ground and Excited State Relaxed Geometries Computed for the Central Fluorene Unit of Different Oligomers[a]

oligomer	α-PF(5)	β-PF(5)	LPPP(5)	γ	spiro-γ/chain 1	spiro-γ/chain 2
$d_{rms} \times 10^3$ (Å)	3.80	3.50	3.48	4.14	0.06	4.31

[a] Changes are calculated as a root-mean-square deviation in the bond lengths $d_{rms} = [\Sigma_{i=1}^{N_d} (d_i^F - d_i^A)^2]^{1/2}/N_d$ where $d_i^A(d^F)$ are the bond lengths at absorption (fluorescence) and $N_d = 16$ is the number of C−C bonds in the central monomer.
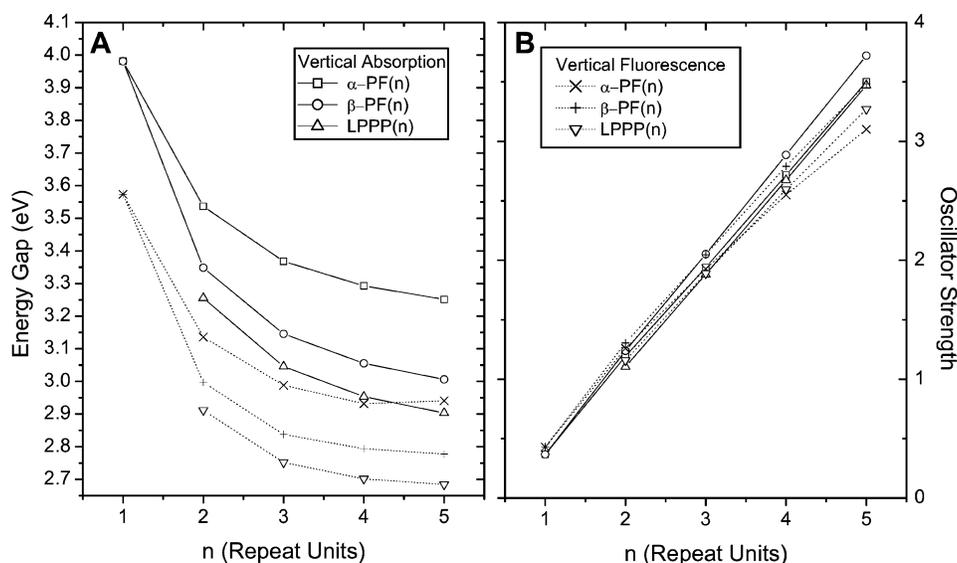
Figure 3. Energy gap scaling with molecular size. (A) Variation of Ω_A and Ω_F, and (B) their corresponding oscillator strengths (CEO/INDO) with the number of repeat units in α- and β-phase PF and in LPPP.

enhancement of conjugation in the β-phase with respect to the glassy conformation is reflected as a 0.24 eV red shift in the vertical absorption frequencies (Table 1). As mentioned above, geometry relaxation along the excited-state energy surface self-traps the exciton in the middle of the chain. At fluorescence the diagonal size L_d of the exciton decreases from 5 to ∼3−3.5 and ∼3.5−4 repeat units in α-PF(5) and β-PF(5) (or LPPP(5)), respectively (Figure 2E′−G′). The exciton self-traps deeper in α-phase PF than in β-phase and LPPP because the large dihedral angles at the extremes of the oligomer in the glassy conformation (Figure 2C) add up extra constrains to the mobility of the excitation, whereas in the planar structures the exciton is only trapped by a local reduction of the bond length alternation. In the case of α-PF(5), molecular relaxation also induces an increase in the off-diagonal exciton size to ∼2−2.5 repeat units due to the enhancement in the local conjugation promoted by planarization of the middle portion of the chain (Figure 2C). This variation in the exciton size is not observed in β-PF(5) and LPPP(5) because their ground-state geometry is already planar. The stronger confinement of the excitation induced by torsional disorder in α-PF(5) is reflected, geometrically, as a larger change in the bond lengths in the central monomer of the chain (Table 2) and, spectroscopically, as a larger Stokes shift (0.3 eV) compared to that of β-PF(5) and LPPP(5) (0.2 eV) (see Table 1).

Overall CEO/INDO/S calculated absorption and emission transition energies show an excellent agreement with experiment (Table 1). The CEO/AM1 approach also reproduces all the experimental trends but with a consistent red shift of all transition energies by ∼0.3 eV. We note that the computed absorption and emission spectra of β-phase PF and LPPP oligomers are nearly identical; the only difference is a slight

red-shift of 0.1 eV for the absorption and emission properties of LPPP with respect to β-phase PF. These results clearly support the hypothesis of a completely planar conformation for the β-phase PF that has been proposed based upon its spectroscopic similarities with LPPP.[13]

The confinement of the cold exciton in the middle of the chain is reflected in the size-scaling behavior of the vertical fluorescence energies and the associated oscillator strengths.[81,82] As shown in Figure 3A, both Ω_A and Ω_F scale roughly inversely proportional to the system size (a characteristic feature of conjugated polymers[81]) and saturate to a constant value in the long-chain limit; α-PF(5), β-PF(5), and LPPP(5) already mimic well the corresponding long-chain values. However, the fluorescence saturates faster than the absorption because the relaxed exciton compromises only a part of the oligomer while the hot exciton is delocalized along the entire chain. This feature shows itself in the behavior of the oscillators strengths (Figure 3B) as a negative deviation from the linear scaling with system size for the fluorescence as compared to the absorption. These deviations are larger in α-phase PF because of the stronger self-trapping of the excitation induced by torsional disorder. A dramatic difference between absorption and emission oscillator strengths can be observed in larger oligomers[83] where the emission from spatially confined photoexcitation does not depend on the chain length.

The computed CEO/AM1 fluorescence spectra for the three oligomers (upper panel in Figure 4) shows a strong vibronic

(81) Hutchison, G. R.; Zhao, Y. J.; Delley, B.; Freeman, A. J.; Ratner, M. A.; Marks, T. J. *Phys. Rev. B* **2003**, *68*, 035204.
(82) Rant, U.; Scherf, U.; Rehahn, M.; Galda, P.; Bredas, J. L.; Zojer, E. *Synth. Met.* **2002**, *127*, 241−245.
(83) Tretiak, S.; Saxena, A.; Martin, R. L.; Bishop, A. R. *Proc. Natl. Acad. Sci. U.S.A.* **2003**, *100*, 2185−2190.
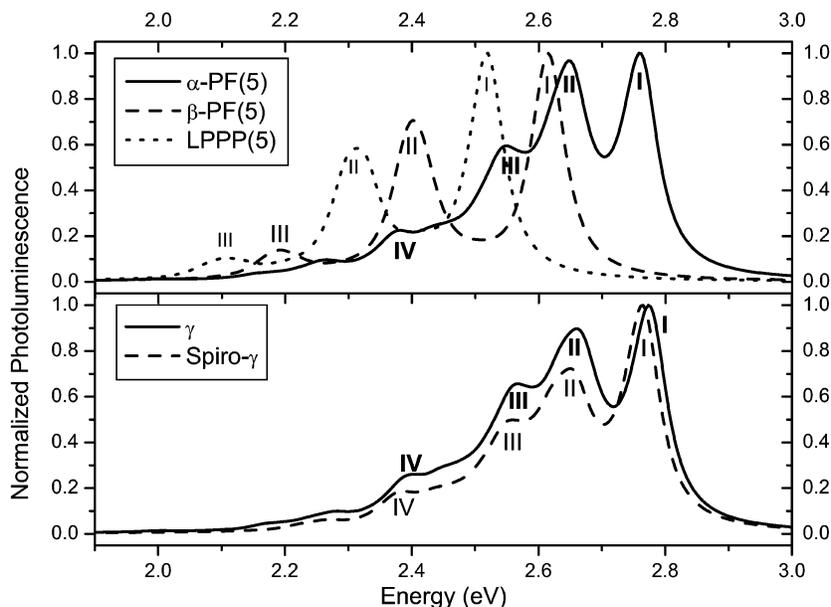
Figure 4. Computed fluorescence spectra (CEO/AM1) for α- and β-phase PF, and LPPP (upper panel) and γ and Spiro-γ oligomers (lower panel). For calculations we assumed an empirical line width of 0.03 eV. The respective experimental values are shown in Table 1.

progression which is characteristic for chains with extended π-conjugation. The structure of the vibronic spectra for all three oligomers has the following features: the 0−0 transition (band I) is the strongest one in both theory and experiment. In addition to homogeneous broadening, the observed broadening of the band may be partially attributed to coupling of the emission to low-frequency vibrational motions ($\sim$100 cm^{-1}) which correspond to torsional and stretching normal modes.[45] Band III in α-PF(5) (II in β-PF(5) and LPPP(5)) is centered 0.21 eV ($\sim$1700 cm^{-1}) to the red from the 0−0 transition, which compares well with the experimental value of 0.18 eV, and originates from the large Franck−Condon factors associated with the bond length alternation vibrational modes (C−C bond stretching, quinoidal motion of benzenes, etc.). Band III in β-PF(5) and LPPP(5) (IV in α-PF(5)) is shifted to the red from the 0−0 transition by $\sim$0.42 eV ($\sim$0.36 eV in experiment) and is merely an overtone of the bond length alternation line. The emissions of β-phase and LPPP oligomers compared to the α conformation are shifted to the red by $\sim$0.2 eV and $\sim$0.3 eV, respectively, which agree well with the experimental trends.[13] Our computed spectra for α-phase PF exhibit a band (II) that is not observed in experiments. It arises due to the coupling of the emission to the normal modes corresponding to swinging motions of vinyl C−H bonds. In experiments, possible solvent interactions and solid-state packing may reduce this degree of freedom and subsequently the magnitude of peak II. We note that our computations are systematically shifted to the red by $\sim$0.3 eV with respect to the experimental values (Table 1) because we are using an AM1 Hamiltonian to compute transition frequencies. Also, due to the semiempirical approximation used for the ground-state potential, our computations typically overestimate the vibrational frequencies.

Figure 5 shows the free dynamics (i.e., using $b = 0$ in eq 5) of α-PF(2) and α-PF(4) oligomers as monitored by geometric and spectroscopic parameters for the first 5 ps after the initial photoexcitation. During this highly nonlinear electron-vibrational dynamics, we observe large scale oscillations in the dihedral angles, the bond length alternation and, as a consequence, the

energy gap. The characteristic time scale in which the central dihedral angle changes sign ("flips") increases with the system size being $\sim$1.5 ps for α-PF(2) and $\sim$4 ps for α-PF(4). As a consequence, this "flipping" observed in α-PF(2) and α-PF(4) is less common for larger oligomers. On the other hand, the quasiperiod of oscillation of the bond length alternation ($\sim$20 fs), determined by C−C stretching vibrational modes, is independent of system size.

We argued before that a localized reduction in the bond length alternation is a characteristic signature of exciton self-trapping. This feature also appears during the free photoexcited dynamics of α-PF(5) (not shown) where we observe that the exciton diagonal size oscillates with an $\sim$20 fs period; i.e., the exciton, initially in a delocalized state, reduces its diagonal size to 3−3.5 repeat units after $\sim$10 fs and returns to the initial delocalized state (4−4.5 repeat units) $\sim$10 fs later. This breathing motion, in which the excitation localizes and delocalizes quasiperiodically, repeats itself during the entire dynamics.[8,83,84] The delocalization (localization) of the exciton always coincides with a maximum (minimum) in the bond length alternation in the central monomer, revealing the strong coupling between electronic and vibrational degrees of freedom in the photoexcited dynamics.

B. Photoexcited Dynamics of Spiro-Linked PFs. In this section, we investigate the effect of spiro-linking on the absorption and fluorescence properties of PF oligomers. Spiro-linking has been studied to prevent π-stacking between the oligomer chains and thus to stabilize the optical properties of PF materials. The spiro chain that we consider (Spiro-γ) consists of two perpendicular α-PF chains joined by the sp^3 carbon at the central fluorene unit of each chain (Figure 6B). The parent chain (γ) is a terfluorene oligomer with phenyl rings in the extremes (Figure 6A).

Figure 6 shows geometric and spectroscopic features of γ and Spiro-γ at absorption and emission. The optical properties

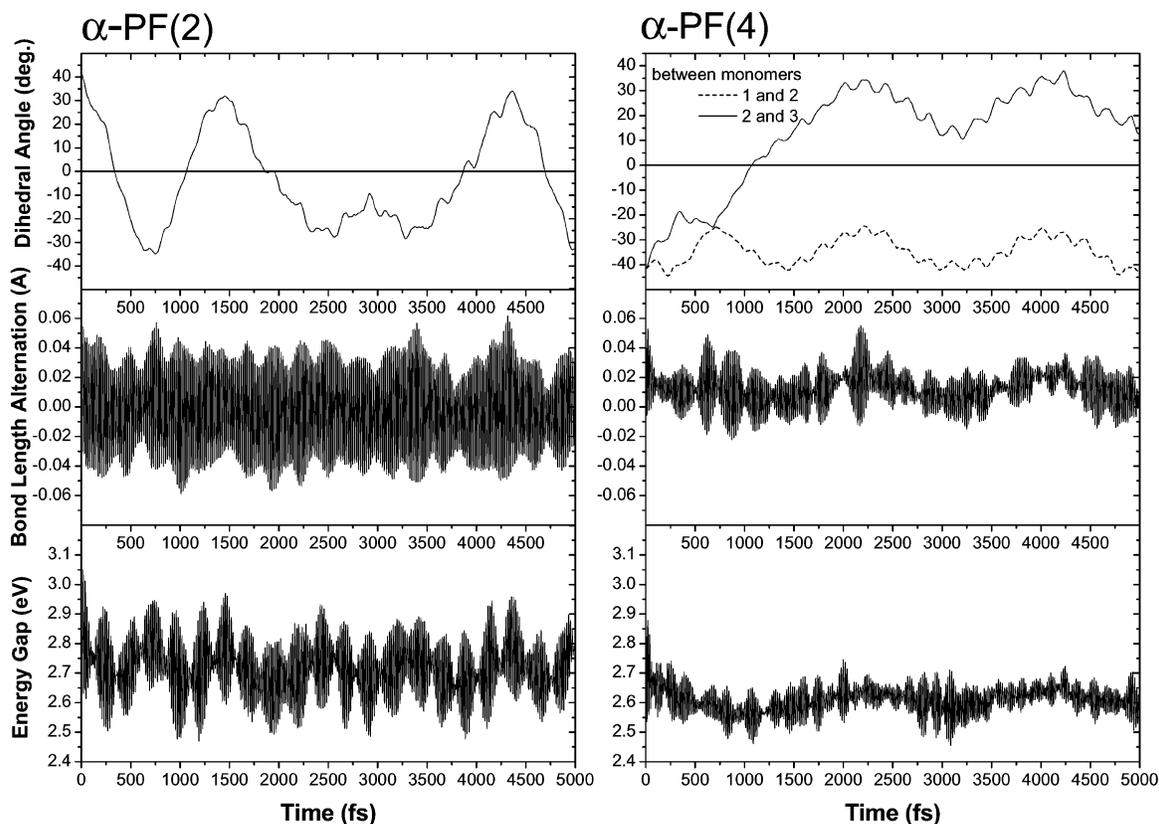(84) Phillpot, S. R.; Bishop, A. R.; Horovitz, B. *Phys. Rev. B* **1989**, *40*, 1839−1855.

Figure 5. Photoexcited dynamics of α-PF(2) (left) and α-PF(4) (right). The plot shows the variation of the dihedral angle, the bond length alternation, and the CEO/AM1 band gap as a function of time. The bond length alternation parameter was measured in the central bond of the oligomers; the dihedral angles are between neighboring fluorene units.

of the unlinked oligomer γ are very similar to that of α-PF(5): the hot exciton is completely delocalized along the chain and self-traps itself after vibrational relaxation (Figure 6E−E′) introducing a 0.36 eV Stokes shift in the vertical transition energies (Table 1). The localization of the excitation is accompanied by a reduction of the bond length alternation and a planarization of the molecule in the middle portion of the chain (Figure 6C and D).

In the ground state, both chains in Spiro-γ have nearly identical geometrical features and closely resemble the α-conformation of the parent chain: dihedral angles of ∼41° between fluorene units and constant bond length alternation for equivalent bonds along the chain (Figure 6C and D). Upon initial photoexcitation, the resulting excited state is completely delocalized between both chains forming a so-called Frenkel exciton. As a result of the negligible coupling between the monomer chains, the first two excited states (I and II) in the Spiro-γ dimer are quasidegenerate being symmetric and antisymmetric combinations of the respective single-chain states (Davydov's pair) (Figure 6F and G). Their associated vertical absorption frequencies Ω_A are basically identical to those of γ (Table 1). Photoexcitation introduces a small coherence between the chains as revealed by nonzero probability amplitude of simultaneously finding an extra electron and a hole in the central fluorene unit of chains 1 and 2, respectively, and vice versa. These appear as nonvanishing off-diagonal elements in the transition densities plots shown in Figure 6F and G. After exciting an electron to the first excited state (Spiro-γ(I)) and subsequent relaxation into the excited-state optimal geometry, we observe self-trapping of the excitation on a *single* chain (Figure 6F′). Structurally this

is reflected as a reduction in the bond length alternation and the dihedral angles (Figure 6C and D) as well as strong changes in the bond lengths of the central monomer of chain 2 (Table 2), whereas chain 1 remains basically unaltered by this process. The resulting structure of chain 2 is essentially identical to the excited-state geometry of γ. These distinct changes in each of the chains composing the Spiro-γ dimer lift the initial degeneracy of the first two excited states: we observe a Stokes shift of 0.36 eV in Spiro-γ(I), equal to the one observed in the unlinked oligomer γ, as opposed to Spiro-γ(II) for which Ω_A remains unchanged (Table 1); i.e., when the excitation associated with the second excited-state confines itself to a single chain, it does not exhibit self-trapping.

A natural transition orbital picture (section II.B) of these phenomena is shown in Figure 7. Upon absorption, both an electron and a hole created by a quantum of light are delocalized along the two conjugated sections of the spiro-oligomer (upper panel). The two NTOs with the greatest weight in the description of this excitation (HOTO → LUTO and HOTO − 1 → LUTO + 1) simply differ by a phase factor reflecting the degeneracy of the first excited state. The TOs to the second excited state (Spiro-γ(II)) in the ground-state geometry are identical to the ones of Spiro-γ(I). In agreement with the transition density analysis (Figure 6), after vibrational relaxation both an electron and a hole are localized on chain 2 for Spiro-γ(I) (middle panels) and on chain 1 for Spiro-γ(II) (bottom panels). Thus, fluorescence comes from recombination of an exciton that is confined on a single chain. Self-trapping of the excitation in Spiro-γ(I), as opposed to Spiro-γ(II), is reflected in the weights of the transition orbitals contributing to each excitation: the most
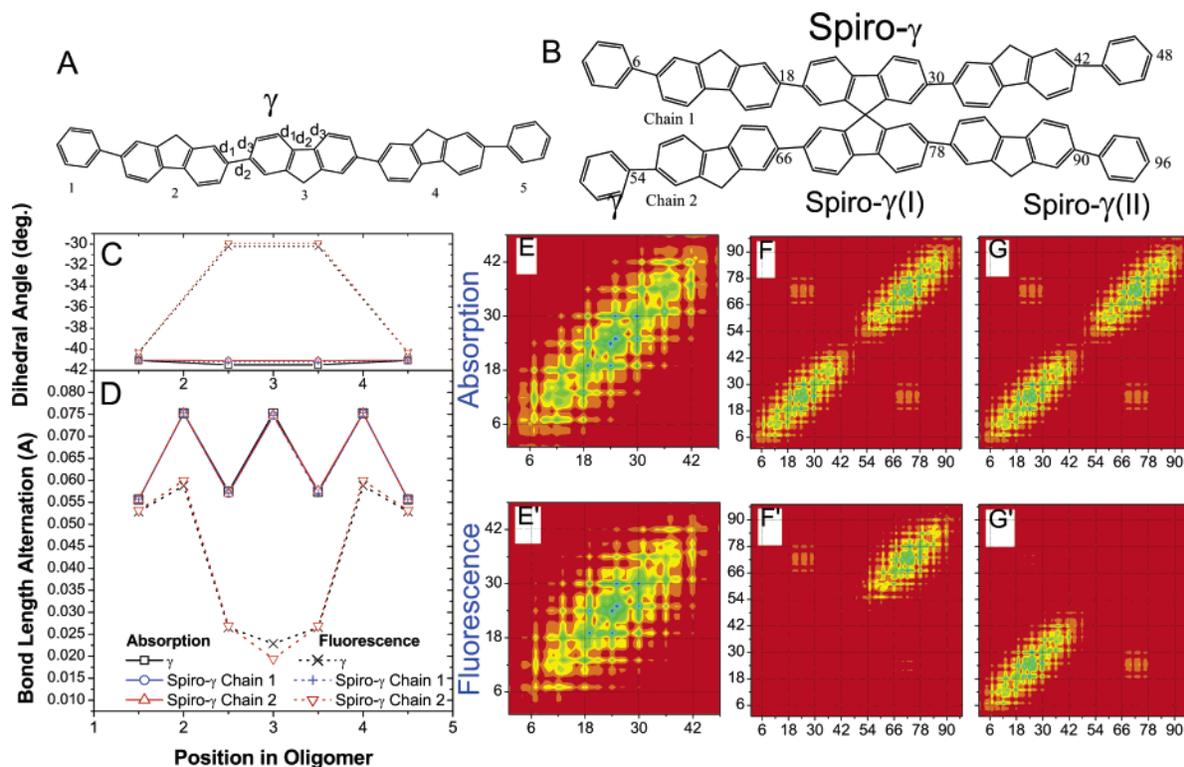
Figure 6. Structure of (A) γ-chain (α-PF(3) oligomer with phenyl rings at both ends) and (B) spiro-linked γ dimer. Parts C and D show, respectively, the variation of the dihedral angle and the bond length alternation (defined in Figure 2) along the chain at absorption and emission for γ and Spiro-γ. The *X*-axis labels consecutive units in the chain as shown in part A (half-integers correspond to the positions between units). Parts E–G show contour plots of the transition density matrices from the ground state (optimal geometry) to the first (^1B_u) excited state (second excited state in the case of part G) for γ and Spiro-γ and correspond to the vertical absorption. Parts E′–G′ show the same quantities as those in parts E–G but at the vertical fluorescence. The axes labels represent the individual atoms in the numbering sequence shown in part B. The color code is shown in Figure 1.
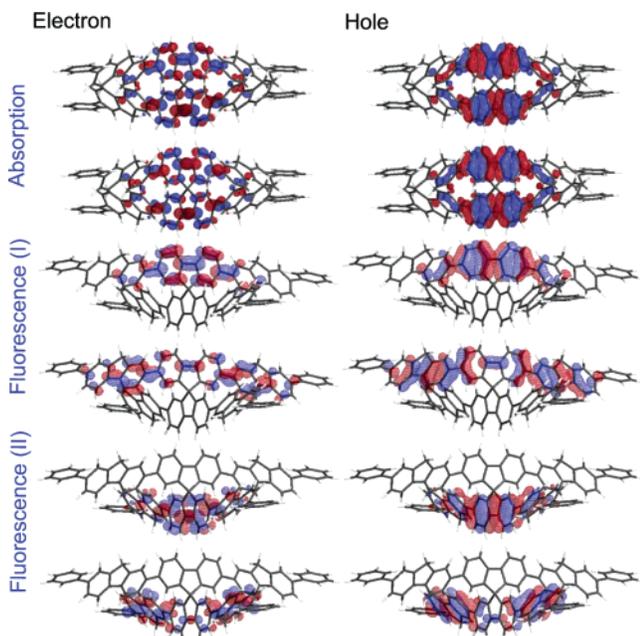

Figure 7. Dominant natural transition orbital pairs contributing to the first two excited states (I and II) in Spiro-γ at absorption and emission. In each plot, chain 2 (see Figure 6B) is at the top. The associated weights (λ) of each NTO pair to the transition density are (from top to bottom) 0.27, 0.25 and 0.66, 0.16 and 0.52, 0.21. These plots constitute an orbital representation of Figures 6F–F′ and 6G–G′.

localized single-particle transition (HOTO $\rightarrow$ LUTO) has a stronger weight in Spiro-γ(I), while the opposite is true for the more delocalized (HOTO $-1 \rightarrow$ LUTO $+1$) NTOs.

The fact that the original delocalized photoexcitation confines itself on a single chain after vibrational relaxation makes the emission properties of spiro-linked oligomers to be very similar to the ones of their single-chain counterparts. This is evidenced in the vertical fluorescence energies (Table 1) and in the fluorescence spectra (lower panel in Figure 4): γ and Spiro-γ have nearly identical fluorescence line shapes. However, Spiro-γ compared to γ shows a small reduction of the intensities associated with the 0–1, 0–2, and 0–3 transitions with respect to the 0–0 band. The structure of the fluorescence spectrum of the spiro-oligomer is the same as the one of α-PF(5) (see discussion in section III.A).

IV. Conclusions

The complex electronic structure of conjugated polymers is reflected in a variety of photophysical phenomena that are exploited in device applications. Modeling of these phenomena constitutes a major theoretical challenge because both electronic correlations (excitonic effects) and coupling to nuclear degrees of freedom (polaronic effects) are essential. The photoexcited dynamics and spectroscopic properties of plastic materials can be characterized using the ESMD methodology described in section II. This method follows adiabatic nuclear trajectories along the molecular excited-state energy hypersurfaces and allows us to obtain excited-state optimal geometries. Even though it is based on a number of approximations (such as the utilization of semiempirical Hamiltonian models and the Born–Oppenheimer approximation), it captures the essential physics of photoexcited "soft" materials with a reasonable compromise between numerical accuracy and computational cost.

In this contribution we have investigated the absorption, emission, and conformational dynamics of photoexcited PFs oligomers of different lengths and in glassy (α), planar (β), and spiro-linked conformations. Our results show that, during the photoexcited dynamics, both slow ($\sim$1 ps) and fast ($\sim$20 fs) nuclear motions couple to the electronic degrees of freedom, inducing large scale oscillations in the energy gap and an exciton breathing motion. In all oligomers considered, the absorption is dominated by completely delocalized excitations, while fluorescence comes from the recombination of self-trapped excitons. The latter phenomenon induces negative deviations in the usual linear scaling of the vertical fluorescence oscillator strengths with the system size. Torsional disorder in α-phase PFs causes a stronger confinement of the excitation at the fluorescence event compared to the planar-type conformations, since both dihedral angles and bond length alternations contribute to this localization. Our computed vertical absorption and emission frequencies as well as the fluorescence line shapes reproduce closely the experimental trends. Our computations show that the emission and absorption properties of spiro-linked PFs are very similar to their single chain counterparts: the "hot" exciton is delocalized along both chains forming a Frenkel-type excitation, while the relaxed exciton is self-trapped on a single chain preserving the emission properties of the parent chain. Thus spiro-linking can be used to prevent π-stacking without compromising the UV−visible properties of PFs.

Exciton self-trapping, the effect of torsional disorder, and the localization of excitations in aggregates are all consequences of the strong nonlinear coupling between electronic and vibrational degrees of freedom during the evolution of photoexcited states. We expect the set of phenomena exemplified by the simulations presented herein to be of common appearance in "soft" materials such as biomolecules, polymers, and proteins.

Supporting Information Available: The geometries (as Cartesian coordinates) of all the stationary points whose excited-state spectra are given in the manuscript and the absolute energies in Hartrees that are computed at these geometries.

JA0489285